ISTITUTO NAZIONALE DI FISICA NUCLEARE

Sezione di Bologna

INFN/AE-90/17
27 Novembre 1990

C. Alvisi, G. Anzivino, F. Arzarello, G. Barbagli, G. Bari, M. Basile, L. Bellagamba, D. Boscherini, G. Bruni, P. Bruni, U. Camerini, G. Cara Romeo, G. Castellini, M. Chiarini, L. Cifarelli, F. Cindolo, F. Ciralli, A. Contin, M. Costa, S. D'Auria, C. Del Papa, S. De Pasquale, F. Fiori, A. Forte, F. Frasconi, P. Giusti, G. Iacobucci, G. Laurenti, B. Lisowski, G. Maccarrone, A. Margotti, T. Massam, R. Nania, V. O'Shea, F. Palmonari, P. Pelfer, R. Pilastrini, S. Qian, G. Sartorelli, M. Schioppa, G. Susinno, R. Timellini and A. Zichichi:

THE ZEUS VERTEX DETECTOR: DESIGN AND PROTOTYPE TEST

Servizio Documentazione
dei Laboratori Nazionali di Frascati

INFN - Istituto Nazionale di Fisica Nucleare
Sezione di Bologna

INFN/AE-90/17
27 Novembre 1990

THE ZEUS VERTEX DETECTOR: DESIGN AND PROTOTYPE TEST

C. Alvisi, G. Anzivino, F. Arzarello, G. Barbagli, G. Bari, M. Basile, L. Bellagamba, D. Boscherini, G. Bruni, P. Bruni, U. Camerini, G. Cara Romeo, G. Castellini, M. Chiarini, L. Cifarelli, F. Cindolo, F. Ciralli, A. Contin, M. Costa, S. D'Auria, C. Del Papa, S. De Pasquale, F. Fiori, A. Forte, F. Frasconi, P. Giusti, G. Iacobucci, G. Laurenti, B. Lisowski, G. Maccarrone, A. Margotti, T. Massam, R. Nania, V. O'Shea, F. Palmonari, P. Pelfer, R. Pilastrini, S. Qian, G. Sartorelli, M. Schioppa, G. Susinno, R. Timellini and A. Zichichi

CERN, Geneva, Switzerland
Dipartimento di Fisica dell'Universita`, Bologna, Italy
Dipartimento di Fisica dell'Universita`, Cosenza, Italy
Dipartimento di Fisica dell'Universita`, Firenze, Italy
Istituto Nazionale di Fisica Nucleare, Bologna, Italy
Istituto Nazionale di Fisica Nucleare, Firenze, Italy
Istituto di Ricerca Onde Elettromagnetiche , CNR, Firenze, Italy

ABSTRACT

A gas vertex detector, operated with dimethylether (DME) at atmospheric pressure, is presently being built for the ZEUS experiment at HERA. Its main design features, together with the performances of a prototype measured at various operating voltages, particle rates, and geometrical conditions on a CERN Proton Synchrotron test-beam, are presented. A spatial resolution down to 35 μm and an average wire efficiency of 96% have been achieved, for a 3 mm gas gap relative to each sense wire.

(Submitted to Nucl. Instrum. Methods)

1. - INTRODUCTION

The HERA machine at DESY[1] (where 820 GeV and possibly 1 TeV protons collide with 30 GeV electrons) is expected to be a very powerful source of electroweakly produced heavy flavours, mainly through the neutral-current boson-gluon fusion mechanism[2,3].

Beauty and charm particles will have a flight path up to a few hundred microns in the $\rho-\phi$ plane, transverse to the beam. In the high-multiplicity environment expected at HERA energies, they can then be identified by reconstructing their decay vertex through a high-precision measurement of the impact parameter D_0, the minimum approach distance between a track and the interaction vertex. Thus, a vertex detector for HERA experiments must satisfy very stringent requirements in terms of spatial resolution, two-track separation, and pattern recognition, with a minimal increase of multiple scattering and photon conversion.

A vertex detector satisfying the above-mentioned requirements has been designed for the ZEUS experiment. It consists of a high-precision drift chamber, with a thin carbon-fibre vessel, and DME at atmospheric pressure as the working gas.

In section 2 the main design characteristics of the detector, which is presently under construction, are presented. The test-beam results obtained with a prototype are given in section 3.

2. - THE ZEUS VERTEX DETECTOR

The ZEUS VerteX Detector (VXD) has to fit into the small space available between the beam-pipe and the Central Tracking Detector (CTD). As schematically shown in fig. 1, its vessel consists of two thin carbon-fibre cylinders. The inner cylinder has a 99 mm radius and is centred on the beam-pipe axis; the outer cylinder has a 159 mm radius and is centred on the beam axis, which is displaced by 10 mm with respect to the beam-pipe axis. The radial length (transverse to the beam-pipe) available for track detection is 36 mm. Notice that the overall radial length free for VXD technology is less than 50 mm. Inside the gas volume, 1.59 m long wires are stretched; they define a set of wedge-shaped cells parallel to the beam-pipe and covering a polar angle region between $\theta = 8.6°$ and $\theta = 165°$. The full azimuthal angle is covered by 120 cells pointing at the beam-pipe centre.

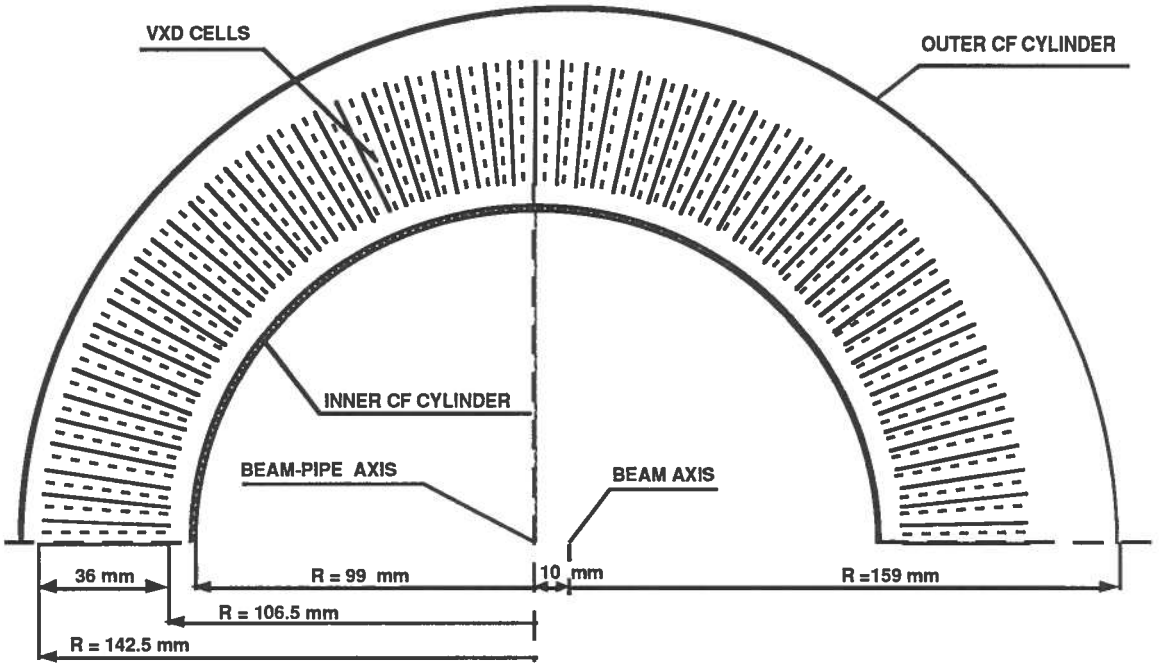

Fig. 1 - Front view (x-y section) of half of the VXD.

2.1 - The gas choice

Following our previous work[4,5], in order to obtain the best spatial resolution, DME at atmospheric pressure has been used. The main physical properties of DME are reported in table 1. In this gas the drifting electrons are thermal even at high values of the electric field (2 kV/cm).

Table 1 - Physical properties of DME	
Molecular weight	46.07
Density	1.918 g/l
Critical temperature	400 °K
Critical pressure	52 atm
Boiling point at 1 atm	-24.9 °C
Vapour pressure at 20 °C	5.24 atm
Flammability limits in air	3.4 ÷ 18 %
Radiation length	4.5×10^{-3} m^{-1}
Primary ionization (m.i.p.s)[a]	55 ions/cm
Total ionization (m.i.p.s)[b]	150 ions/cm
Ion mobility[b]	0.056 $\mu m^2/V$ ns

(a) F. Sauli, CERN-LAA/89-1.
(b) Our measurement.

Consequently, their drift velocity is low (5 μm/ns), thus allowing for high spatial resolution even with a moderate resolution in the drift-time measurement. Moreover, DME has better quenching properties than other cool gases.

However, since the electrons are thermal, i.e. the drift velocity is non-saturated, the electric-field configuration of the drift cell and the gas pressure must be precisely known.

2.2 - The cell configuration

The cell, schematically shown in fig. 2, is defined by three radial wire planes: a central plane consisting of 13 field wires alternated with 12 sense wires, and two lateral planes made of 25 drift wires each. The angle between planes is 1.5°, giving a drift space of 2.6 to 3.6 mm going from the inside layer of wires towards the outside one. The wire spacing is 1.5 mm in any plane, giving a 3 mm gas gap relative to each sense wire. The wires are made of gold-plated tungsten and their diameters, mechanical tensions, and working voltages are listed in table 2.

The electrical scheme for the drift wires is shown in fig. 3. In order to get the same drift velocity for all the

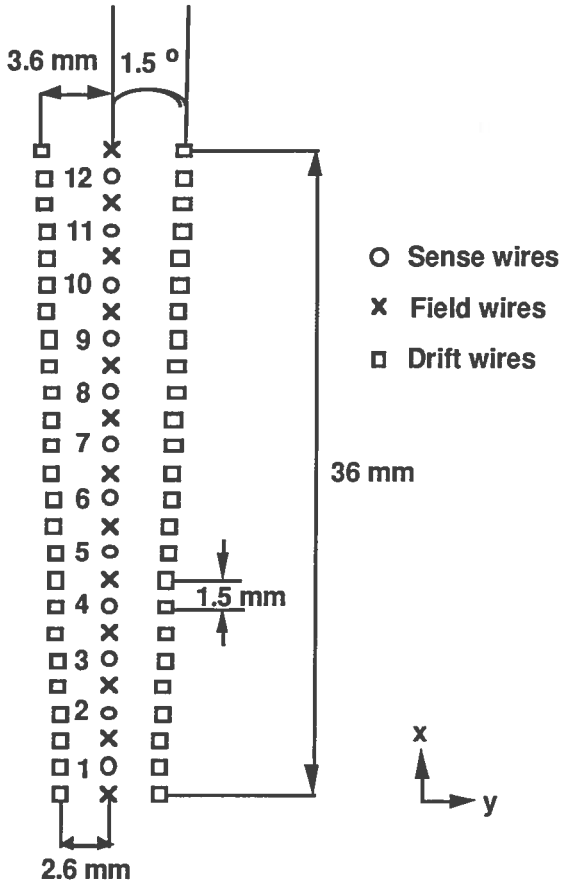

Fig. 2 - Drift-cell geometry.

Table 2

Wires	Diameter (μm)	Mechanical tension (g)	H. V. (V)
Sense	20	50	0
Field	50	200	-2150
Drift	50	250	-2000 ÷ -2200

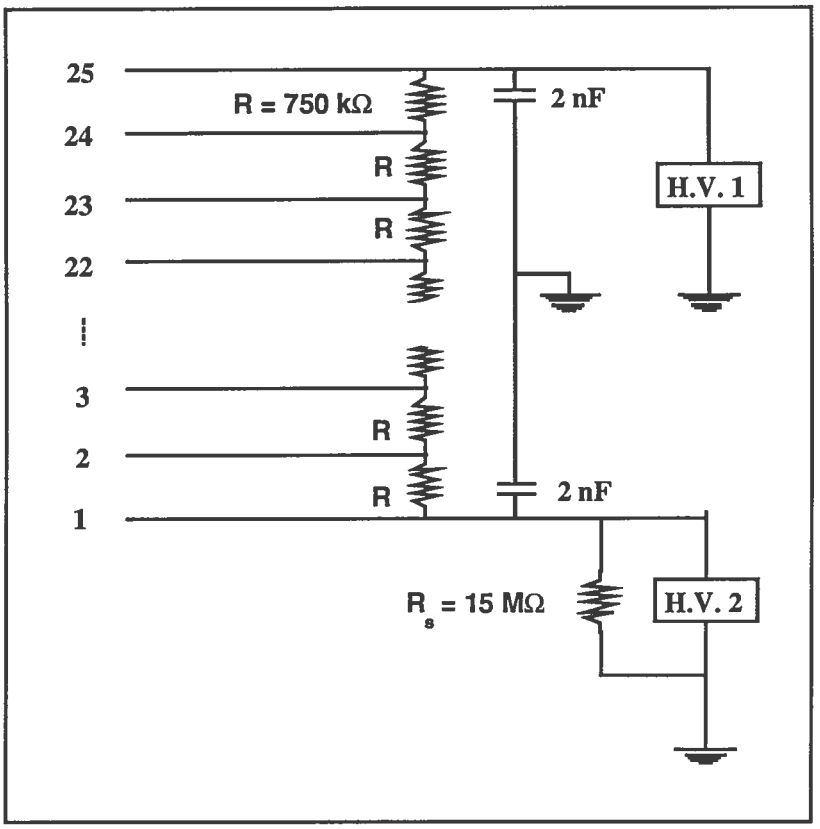

Fig. 3 - Electrical scheme for the drift-wire circuit.

12 sense wire layers in the region where the wire time-to-distance relation (TDR) is linear, the drift voltages are graded with hybrid resistor chains with a step $\Delta V = 8$ V.

A typical wire TDR, for a wire positioned at half the cell height, is presented in fig. 4, whilst the equipotential, field, and drift lines relative to the cell are shown in fig. 5. All quantities have been calculated using the simulation programme of ref. (6).

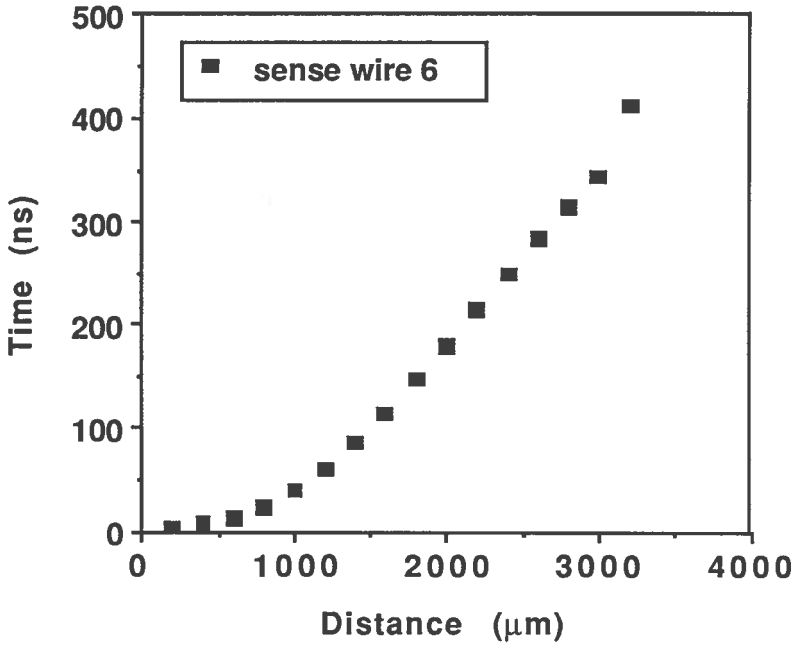

Fig. 4 - Time-to-distance relation relative to sense wire 6.

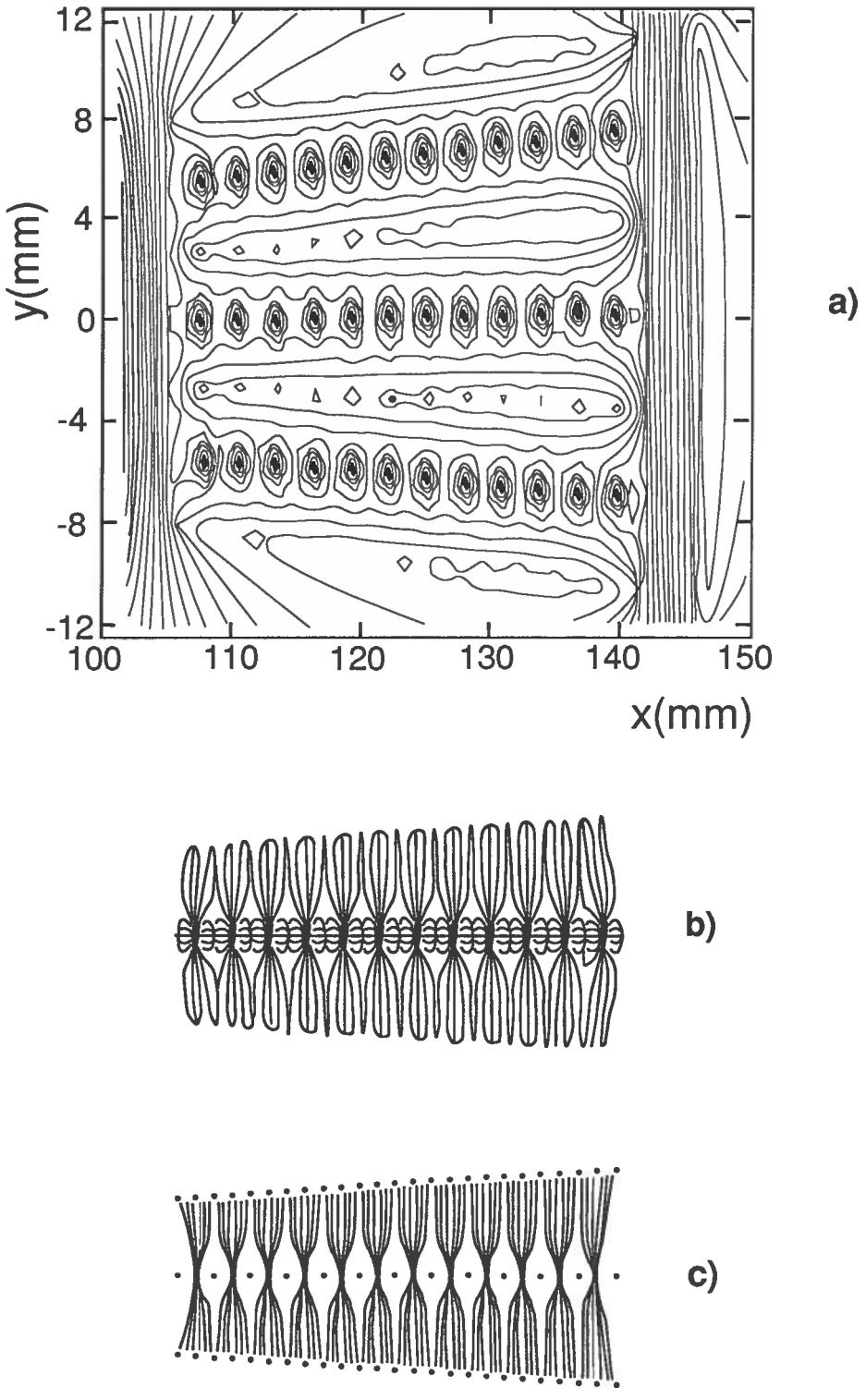

Fig. 5 - Equipotential lines (a), field lines (b), and drift lines (c), inside the drift cell.

2.3 - The mechanical design and mounting procedure

To accommodate the very large number of wires (6000) inside the VXD, we have adopted a modular technique. This gives the possibility of checking the mechanical and electrical parameters of each module before mounting it on the detector, and to replace easily a faulty or broken module.

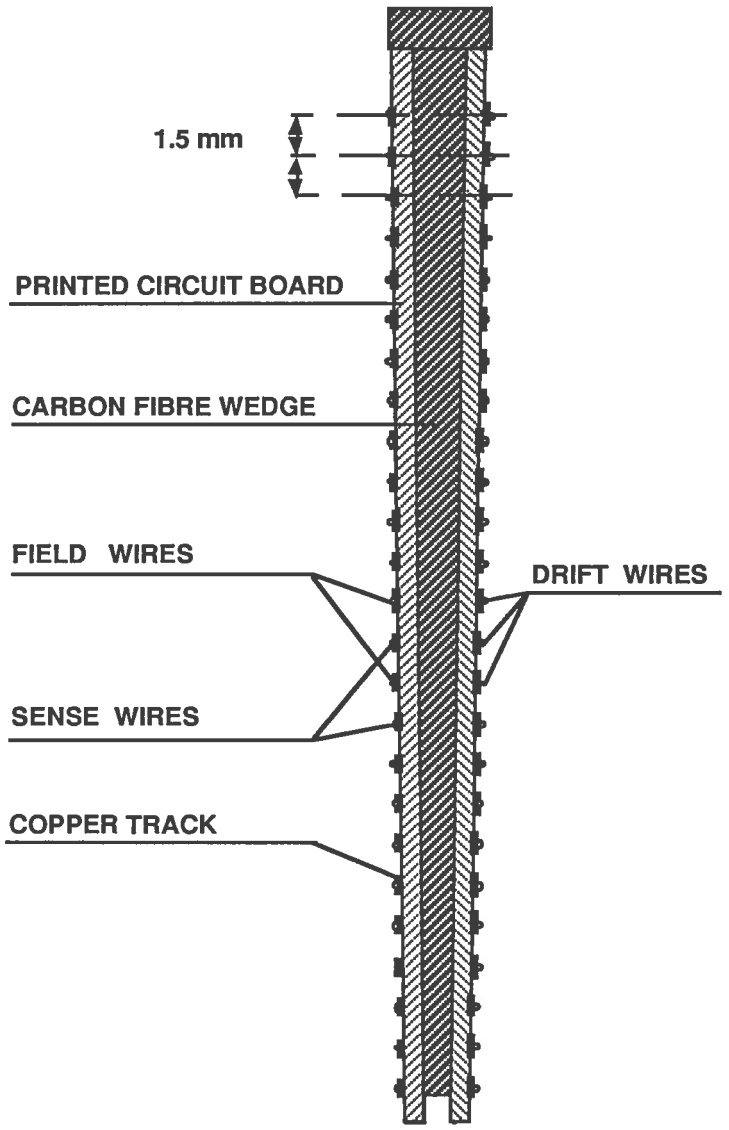

Fig. 6 - Section of a CF wedge with PCB and wires on it.

Each module (fig. 6) consists of carbon fibre (CF) wedges on both sides of which G10 printed circuit boards (PCB) are glued. One of them carries the field and sense wires, the other one the drift wires. The resistive hybrid chains and the Kapton flat cables for signals and HV supplies are also carried by the two PCBs. To prevent electrostatic instabilities, wires are supported every 40 cm by Delrin spacers glued to them.

The modules are mounted on the end flanges, built in the shape of cog-wheels (fig. 7), where the teeth of the CF wedges engage the cut-outs between two adjacent cogs, thus remaining locked in position. The compressive load (1134 kg) is supported by the inner CF tube (1.2 mm thick). An external CF tube (0.72 mm thick) and two flanges complete the gas vessel.

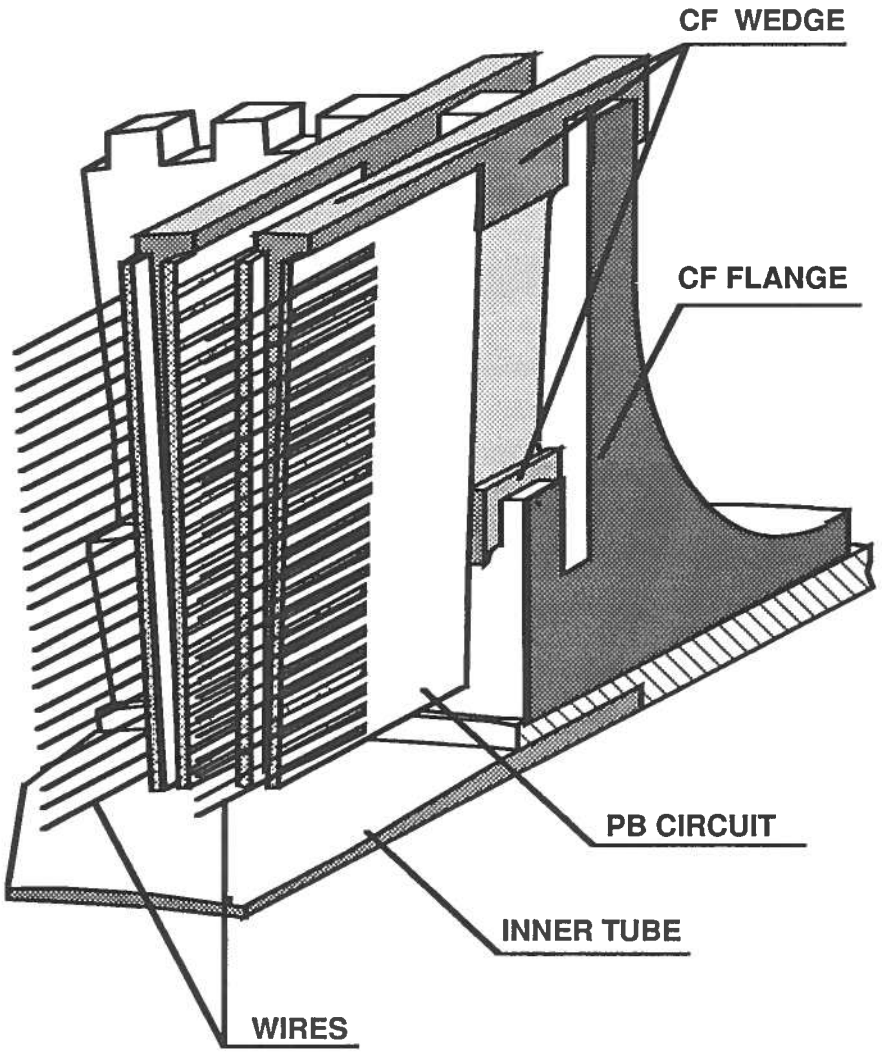

Fig. 7 - A schematic drawing of the prototype CF cog-wheel with a wedge mounted on it.

Particular care has been taken to minimize the thickness of material traversed by particles. For this reason, in the outgoing proton region, where a high flux of particles is expected, a CF flange is employed, whilst all the electrical connections and feedthroughs are placed at the other end of the vessel. In the final detector, the surfaces of both cylinders and of the flange in contact with the gas will be coated with a layer of Cu and one of Au (50 μm and 2 μm thick, respectively) for electromagnetic and synchrotron radiation shielding. The total thickness at $\theta = 90°$ is only 1% of one radiation length X_0.

3. - PROTOTYPE TESTS

3.1 - Test set-up

The test prototype consists of five cells, built according to the mounting procedure described in section 2.3, the only difference being that there is an active wire length of 1 m. A picture of the prototype is shown in fig. 8.

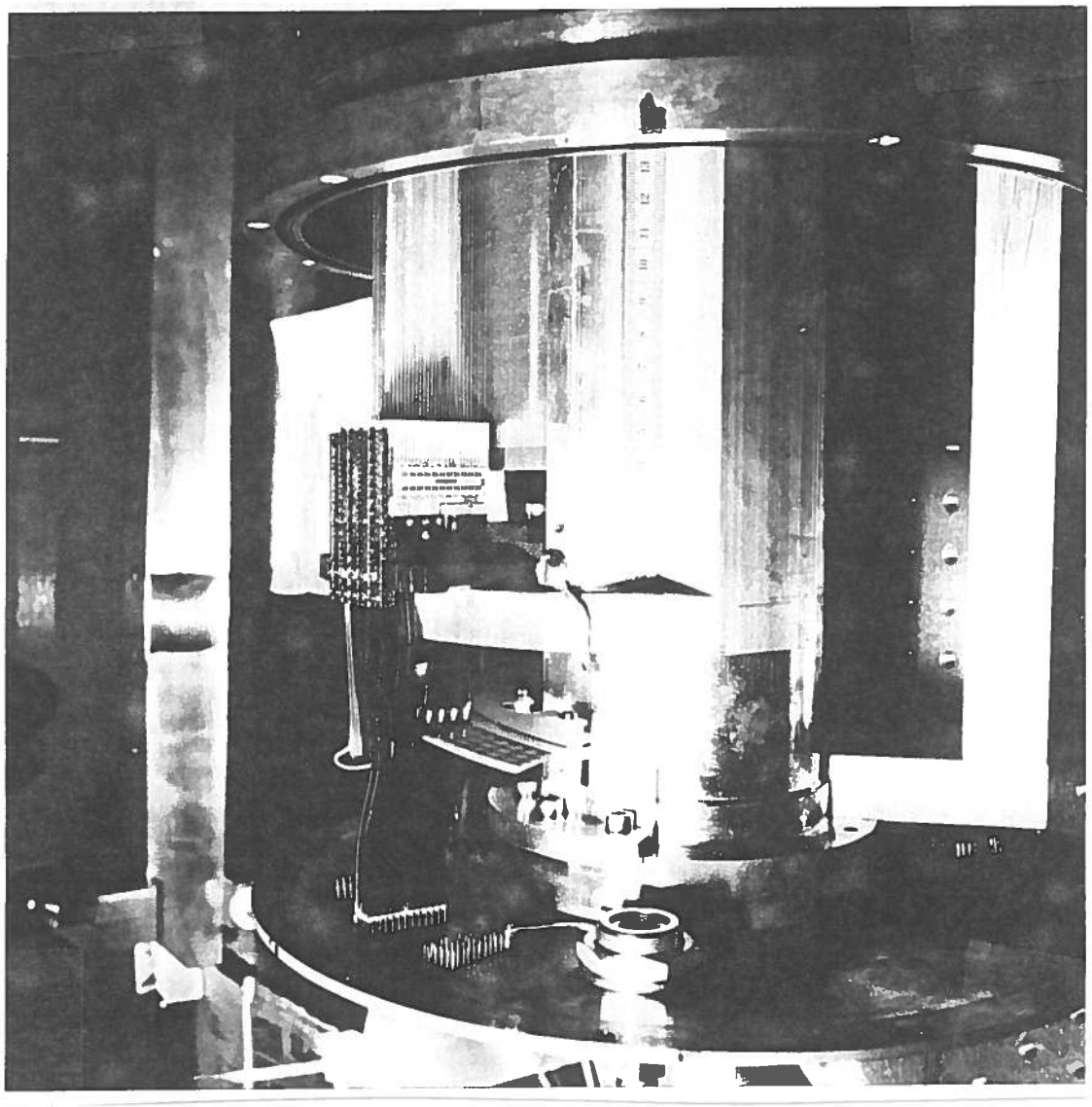

Fig. 8 - Photograph of the final prototype, showing signal and HV connections.

The accuracy in wire positioning has been measured by metrological survey; with reference to fig. 2, for each plane of wires the resulting r.m.s. of the fit residuals were $\sigma_x = 20$ μm and $\sigma_y = 15$ μm.

The prototype has been tested at the CERN PS with a secondary beam of 6 GeV/c pions and electrons. The experimental set-up is shown in fig. 9. The trigger was given by the coincidence of three scintillation counters defining an area of 3×35 mm^2, and covering mainly the central cell among five. The front-end electronics[+)] and the signal-cable type and length were as foreseen for the ZEUS experiment. The readout electronics consisted of a standard discriminator, followed by a 1 ns least significant bit TDC.

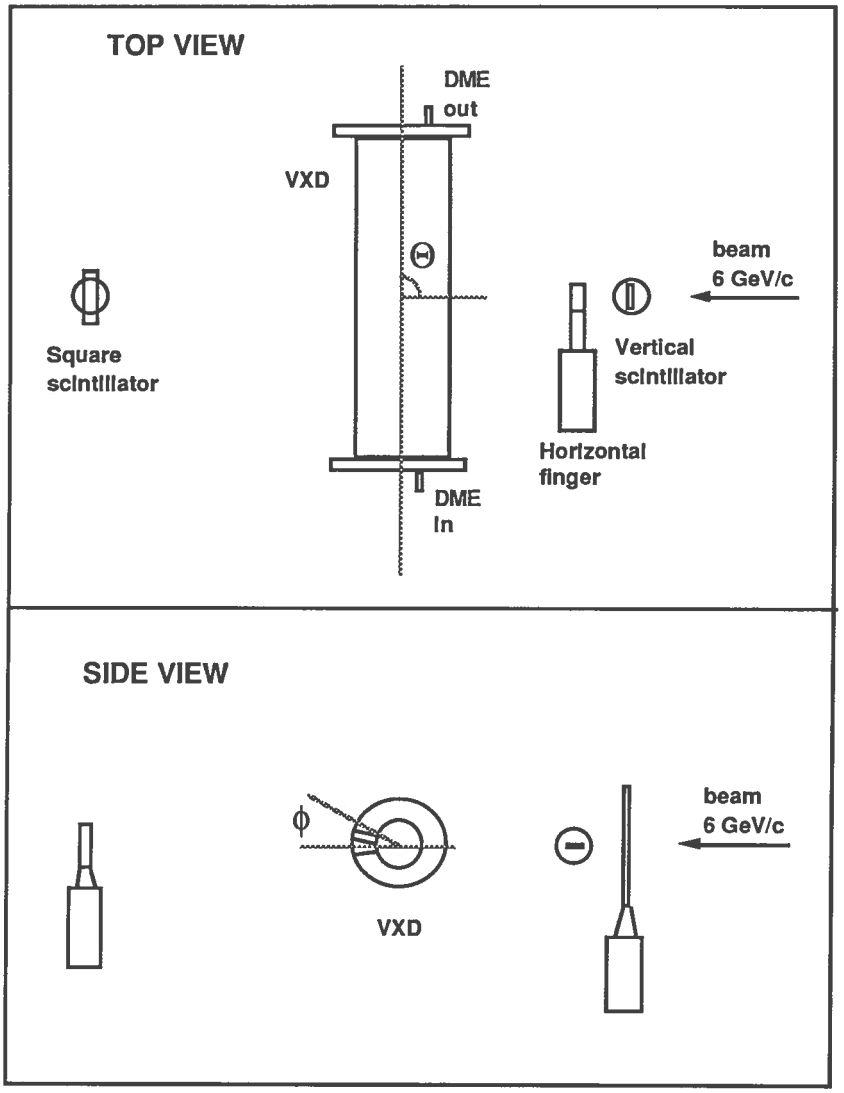

Fig. 9 - Sketch of the set-up used in the CERN PS test beam.

[+)] The front-end electronics, consisting of a preamplifier and a shaper, has been developed and built by the Siegen University group[7].

Data have been taken at different gain voltages and rates, and under different geometrical conditions: the VXD prototype behaviour as a function of ϕ and θ angles (see fig. 9) has been tested, as well as the rate capability and the uniformity in the wire direction (z).

The double-track separation has also been measured, by selecting electrons with a Cherenkov counter, and by adding a 1 X_0 lead plate in front of the detector. A multihit TDC has been used in this case.

The gas gain has been measured for different voltages, by recording charge spectra. Furthermore, different incident track angles have been used in order to check the linearity of the 'charge' response as a function of track length. This allows the absolute gain to be evaluated.

3.2 - Data analysis

A typical TDC spectrum is shown in fig. 10. The drift distances, i.e. hit positions, are obtained by linear interpolation, using the TDRs calculated for each wire.

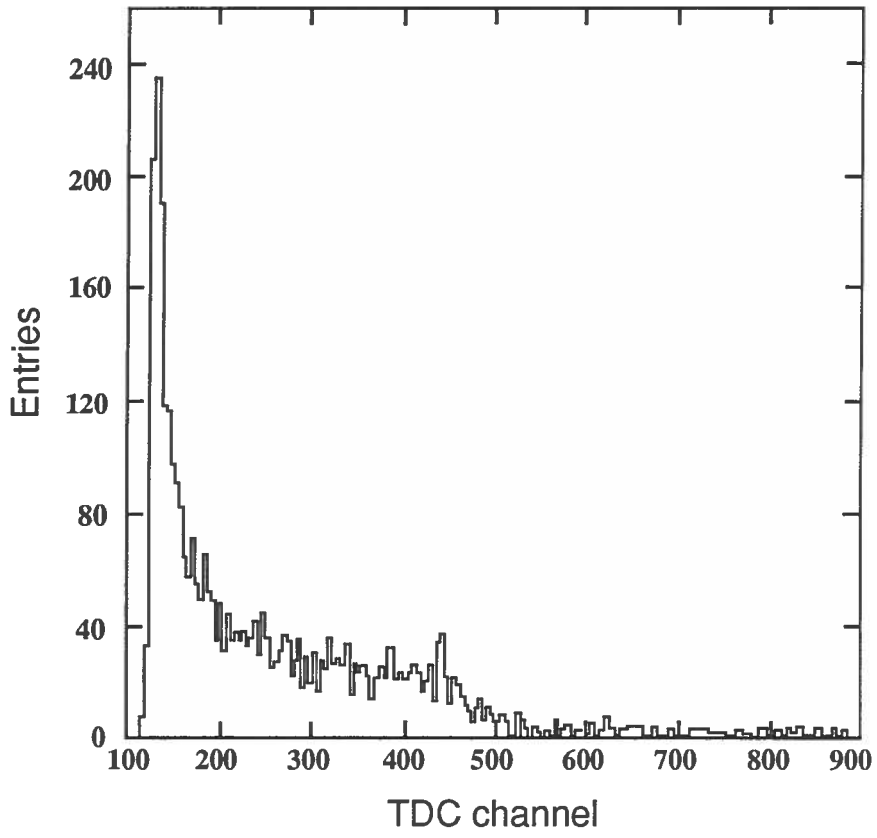

Fig. 10 - A typical drift-time spectrum. The shape of the spectrum is related to the electron drift velocity as a function of the distance from the sense wire.

A 'road' method algorithm has been used for track finding, with a road width dependent on the cell region: 220 μm near the sense wire, 140 μm in the central region, and 500 μm near the edge of the cell. As discussed later, this choice is a good compromise between efficiency and resolution, and corresponds to a road width 4 times the error on the measured points. This error is given by $\sqrt{\sigma_I^2 + (t_w w_d)^2/12}$, where σ_I is the expected intrinsic resolution, t_w the TDC time resolution, and w_d the calculated drift velocity. Only candidates with more than 4 hits inside the road have been fitted as straight lines. The left-right ambiguity has been solved by requiring a constant track slope throughout the detector. The candidate with the highest hit multiplicity has been retained.

The efficiency and the resolution, relative to the central cell, have been evaluated in various experimental conditions. The wire efficiency has been defined as the actual number of hits of the reconstructed tracks, divided by the number of geometrically expected hits. The resolution has been calculated in two ranges of distances from the sense wire (smaller and larger than 1200 μm) as the FWHM/2.35 of the residual distribution. Figure 11 shows the residuals for distances larger than 1200 μm. Neither wire alignment nor correction for track inclination have been introduced in

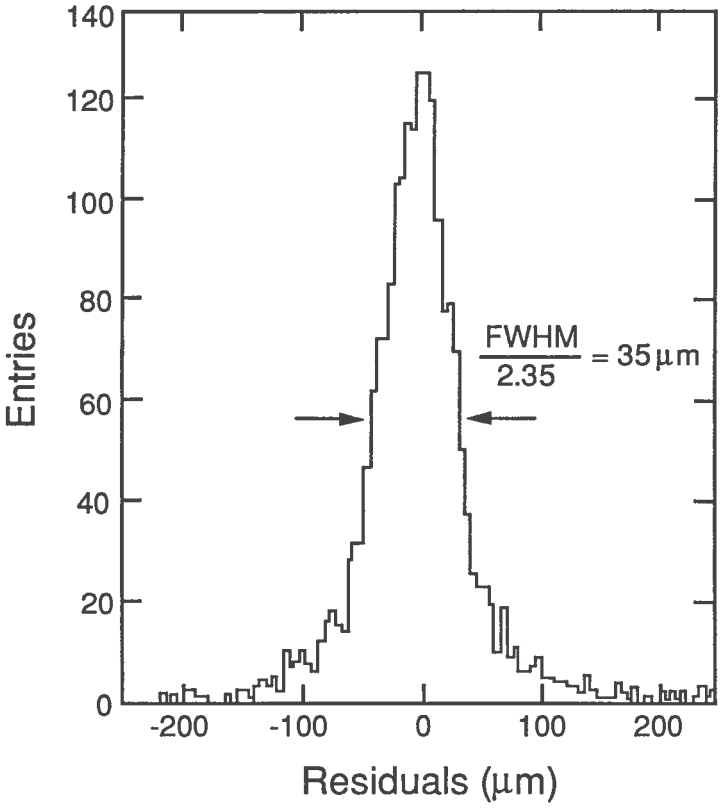

Fig. 11 - Residual distribution, relative to sense wire 11, for distances $d > 1200$ μm from the wire.

this analysis. Notice that, owing to a bad contact in the central cell, wire 10 was found to be inefficient, and therefore discarded. An example of a reconstructed track inside the detector is shown in fig. 12.

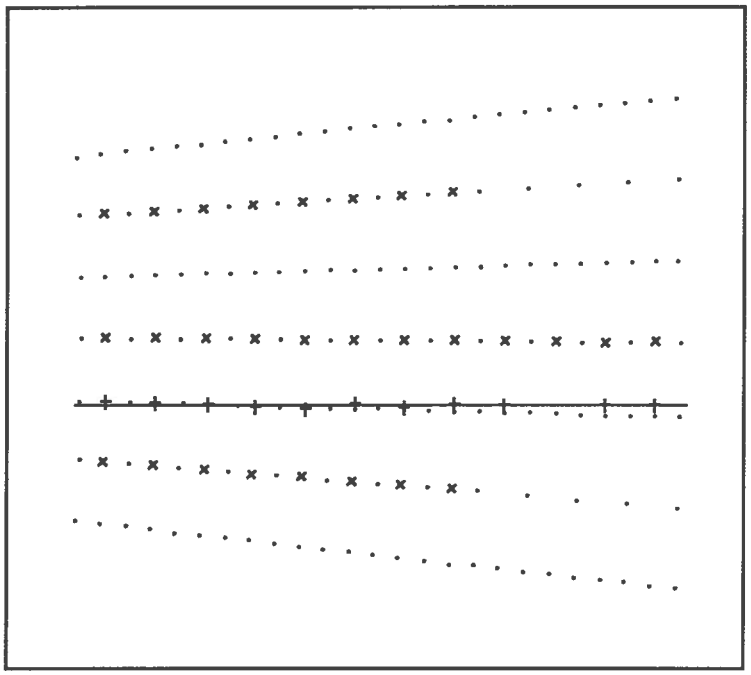

Fig. 12 - Graphic display of a track reconstructed inside the VXD prototype. The crosses represent the sense wires read-out. Not all the sense wires were electronically instrumented in the nearby cells, while the central cell was fully instrumented.

3.3 - Results

In fig. 13 the measured gas gain as a function of the electric field on the wire surface is reported. It has been obtained (see section 3.1) by linear fit of the peak position of the charge spectra as a function of the track length inside the detector. Different track lengths are obtained varying the incident angle.

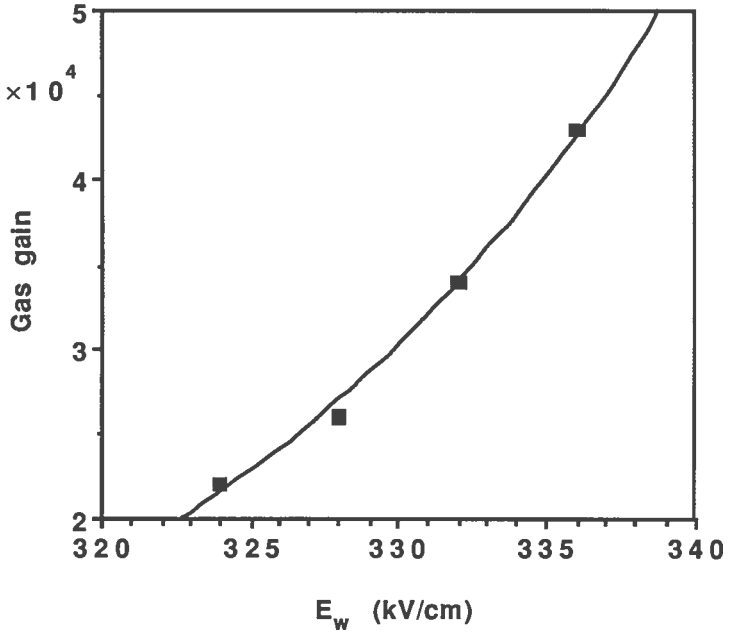

Fig. 13 - Gas gain plotted against electric field on the sense wire surface. An exponential fit is superimposed.

The efficiency as a function of the gain voltage, for fixed drift field, is shown in fig. 14a. The resolutions close to and far from the sense wires, obtained under the same conditions, are shown in fig. 14b. The values reported are averaged over all the wires. At the chosen working point, $V_g = 2150$ V, the efficiency is as high as 96%, despite the small gas gap between the wires

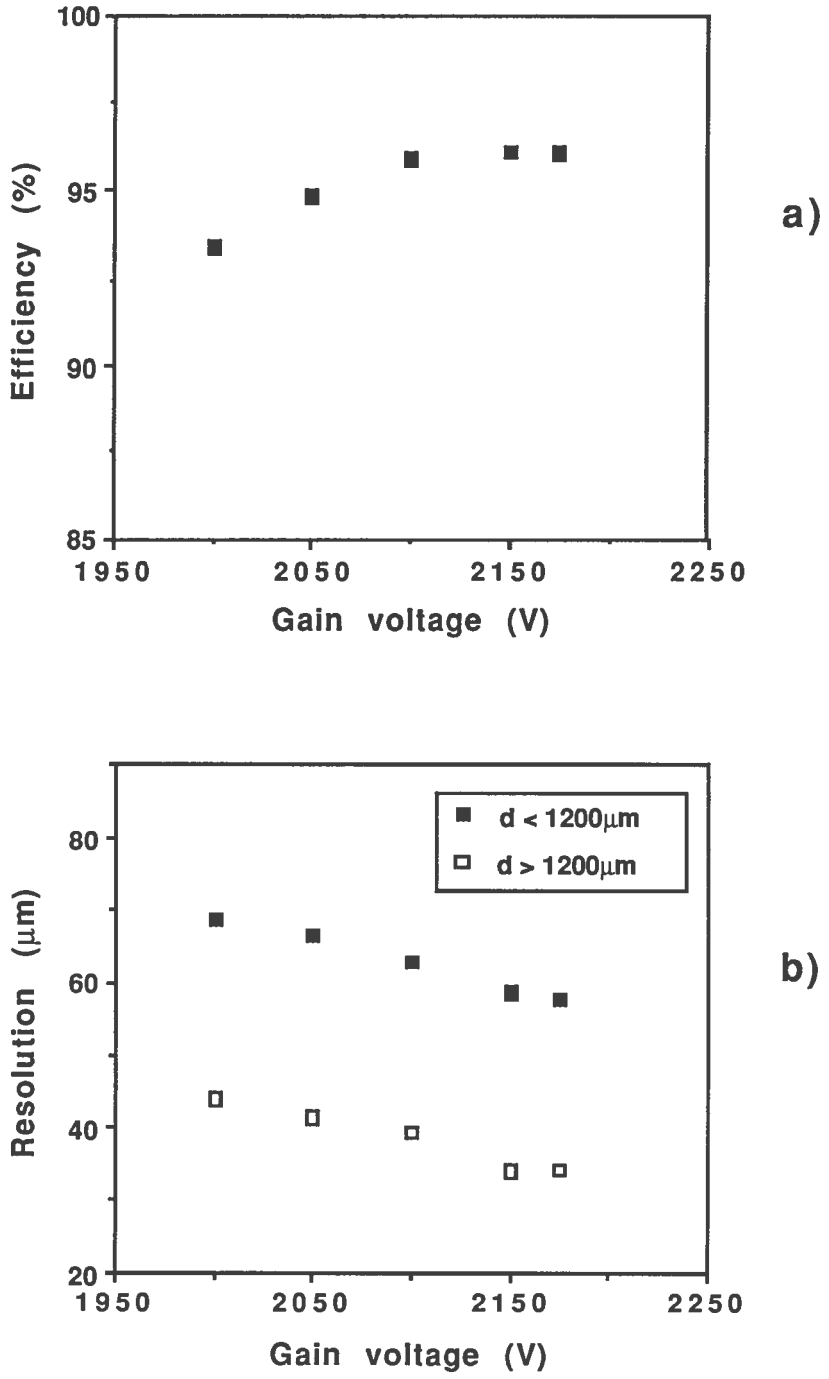

Fig. 14 - efficiency (a) and resolution (b) as a function of gain voltage, averaged over all the wires.

(3 mm). A variation of ± 1 σ of the road width affects the efficiency and the resolution less than 2% and 3% respectively. The resolution dependence on the drift distance relative to wire 11 is shown in fig. 15; in the central drift region, a resolution of 35 μm is obtained, with degradation near to the sense wire and far away from it, i.e. near to the cell edge.

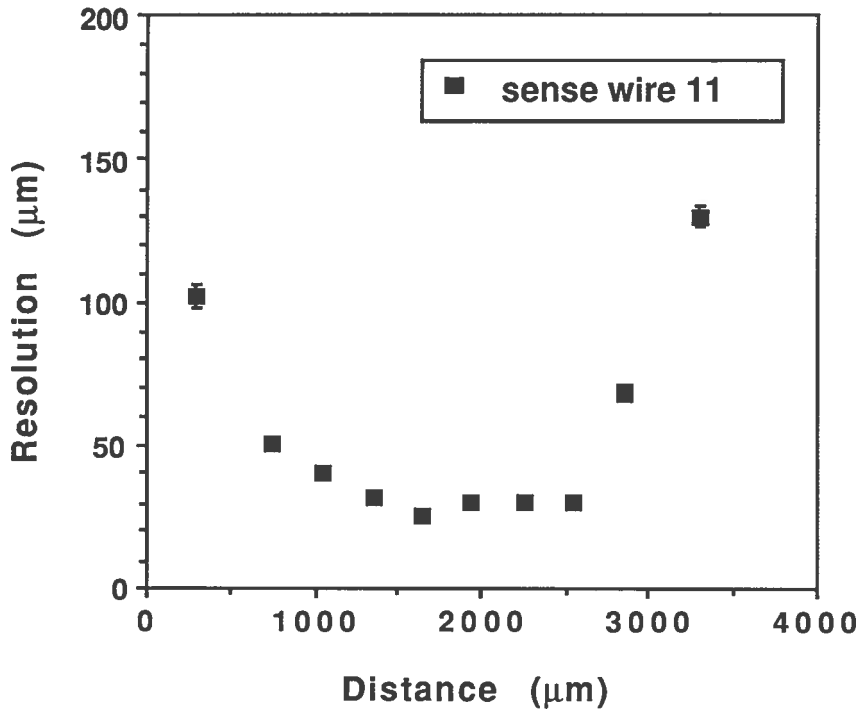

Fig. 15 - Resolution as a function of drift length relative to sense wire 11.

The chamber has been tested up to a rate one order of magnitude higher than that expected at HERA, including backgrounds. Only a slight reduction of the efficiency as a function of the rate has been found (fig. 16a). No appreciable variation of the resolution has been observed within the explored range (fig. 16b).

The VXD prototype performances (efficiency and resolution) as a function of the polar (θ) and azimuthal (ϕ) angles, and of the position z along the wire direction are shown in figs. 17, 18, and 19, respectively. While the behaviour of the detector is independent of θ and z, a 5% efficiency reduction and a variation of the resolution have been found as a function of ϕ. It is straightforward to eliminate this effect via the angle-dependent TDR.

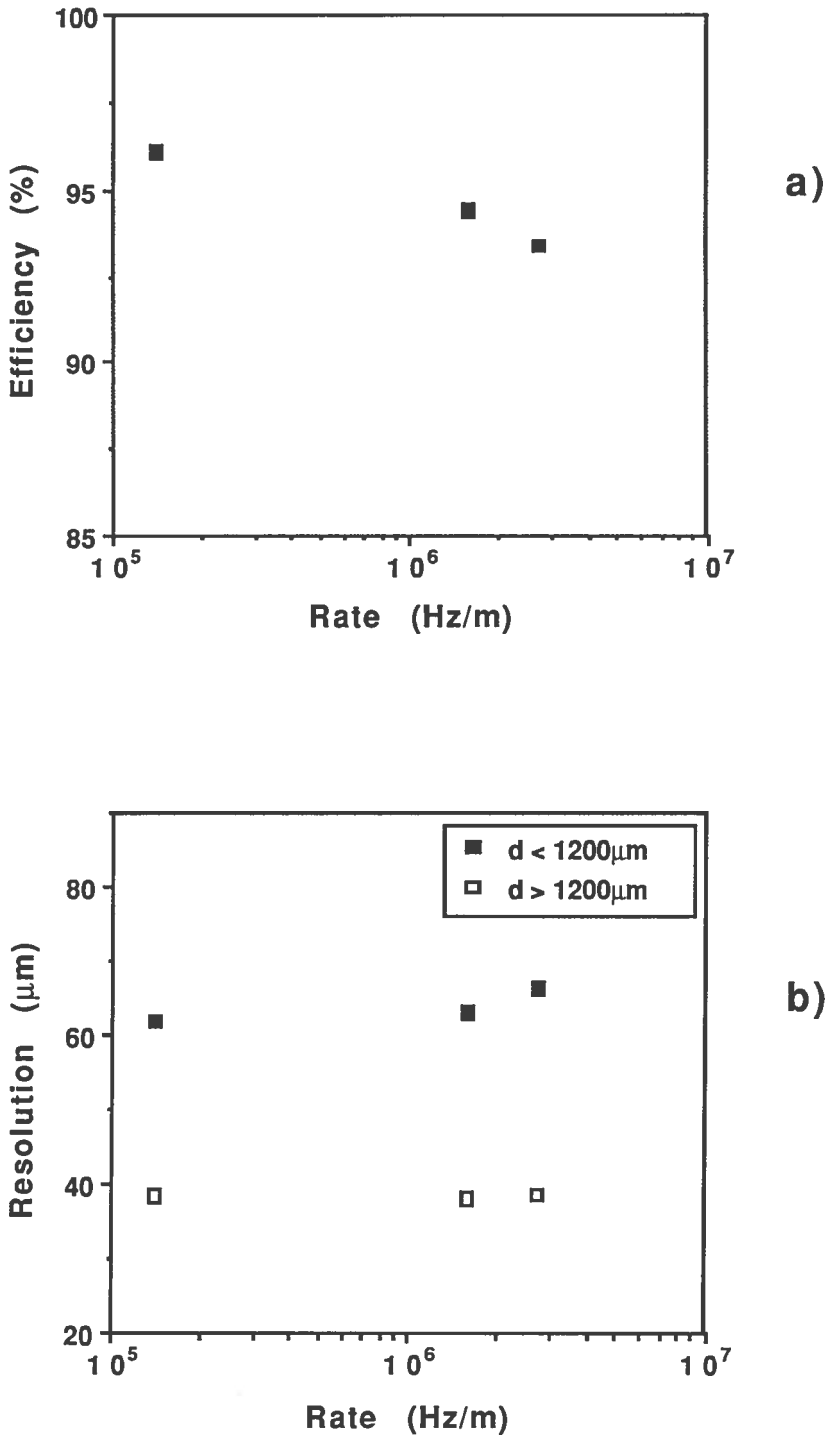

Fig. 16 - Efficiency (a) and resolution (b) as a function of rate, averaged over all the wires.

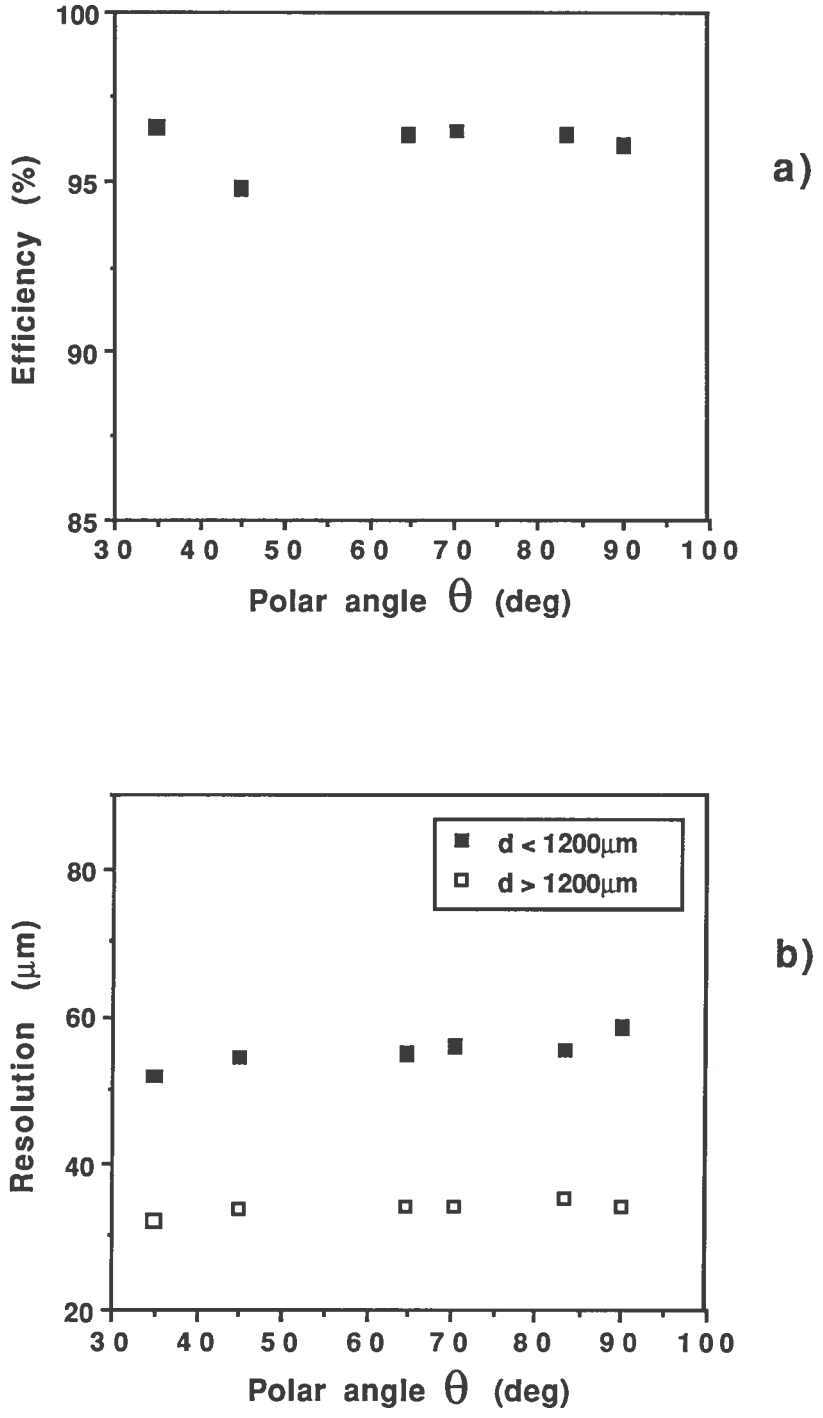

Fig. 17 - Efficiency (a) and resolution (b) as a function of polar angle θ, averaged over all the wires.

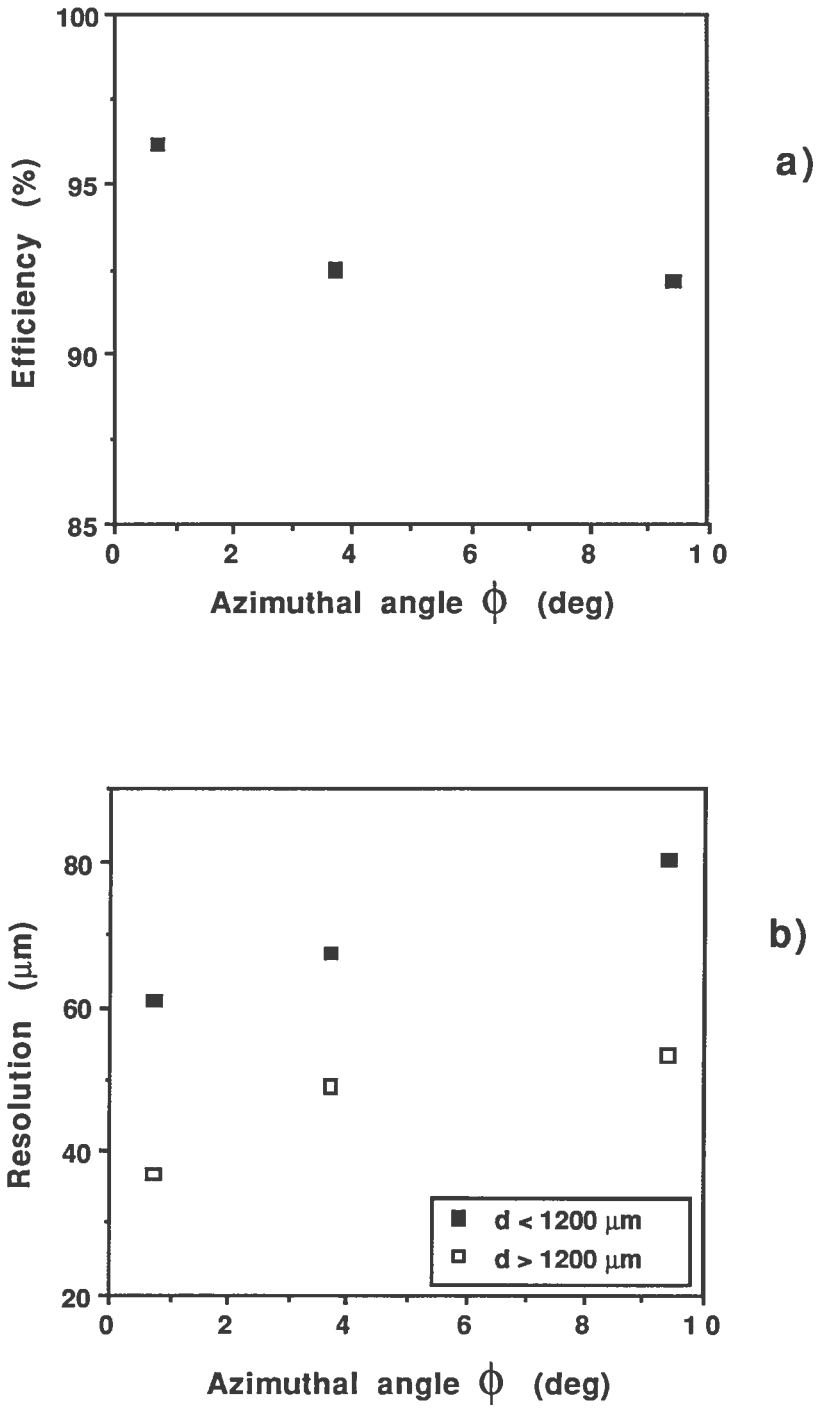

Fig. 18 - Efficiency (a) and resolution (b) as a function of azimuthal angle ϕ, averaged over all the wires.

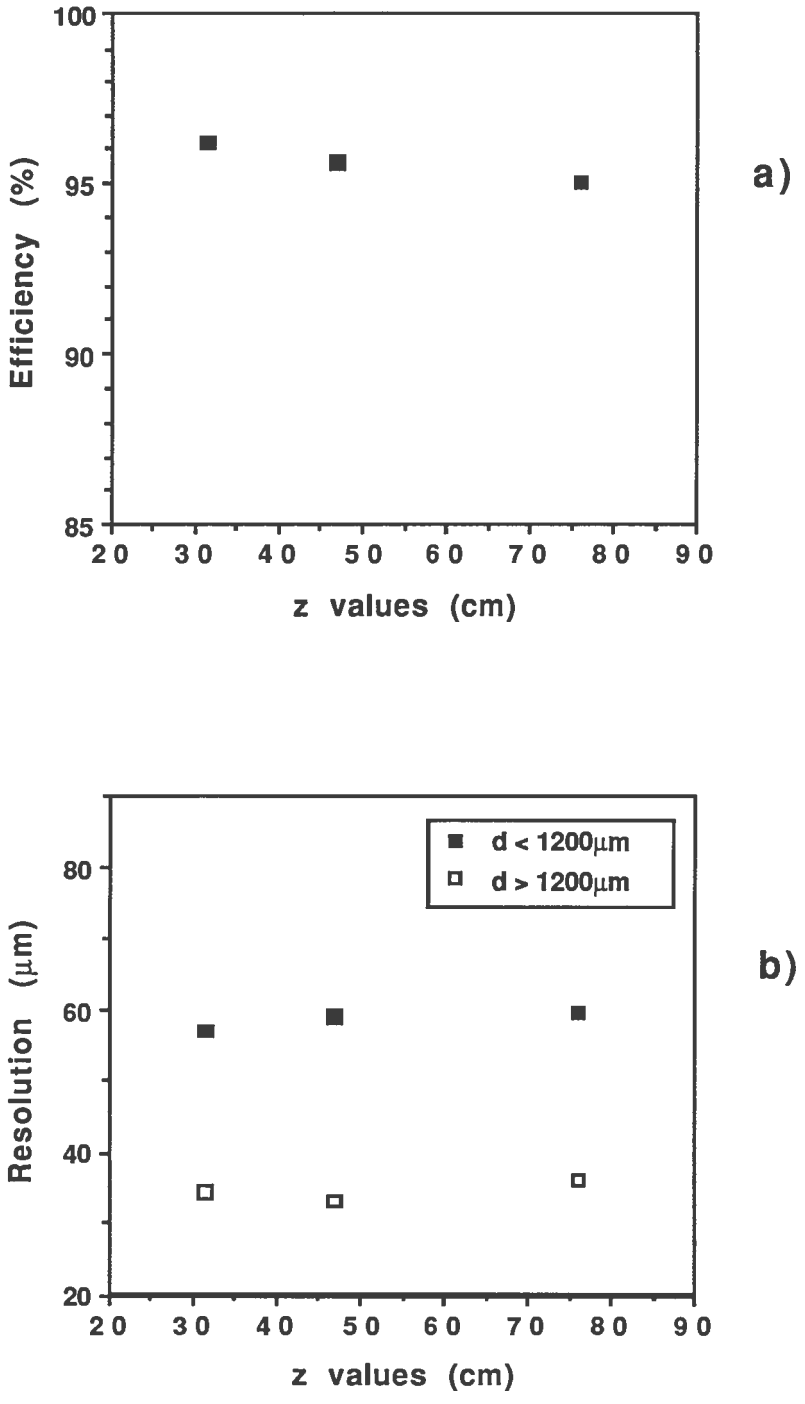

Fig. 19 - Efficiency (a) and resolution (b) as a function of *z*, averaged over all the wires.

Figure 20 shows the efficiency and the resolution as a function of wire number, relative to the central point of fig. 19. The results obtained are shown with 1 ns and 4 ns TDC time resolution. The grouping of the TDC channels is done at 4 ns in order to simulate the TDC resolution of the final VXD readout electronics[8]. No significant difference with respect to the 1 ns case is observed.

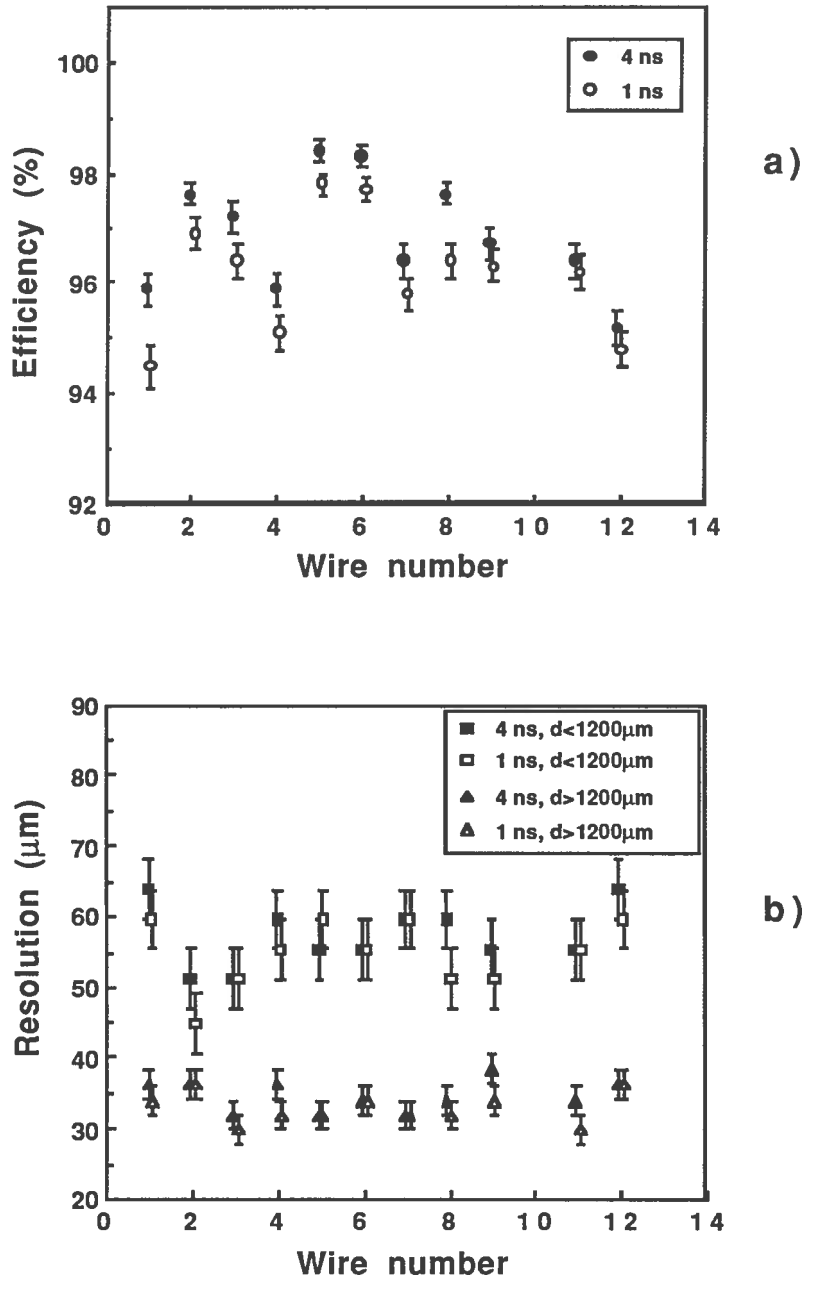

Fig. 20 - Efficiency (a) and resolution (b) for the single wires of the central cell for 1 ns and 4 ns TDC bin width.

The possibility of reconstructing two tracks in the same cell has also been investigated, taking into account pairs of tracks, with a hit point multiplicity greater than 5 for each track. The minimum reconstructed distance between two hits on wire 11 is reported in fig. 21 as a function of the distance from the wire of the first hit. The resulting double-hit separation is about 1200 μm close to the sense wire, 900 μm close to the cell edge, reaching 600 μm in the slow drift velocity region of the cell.

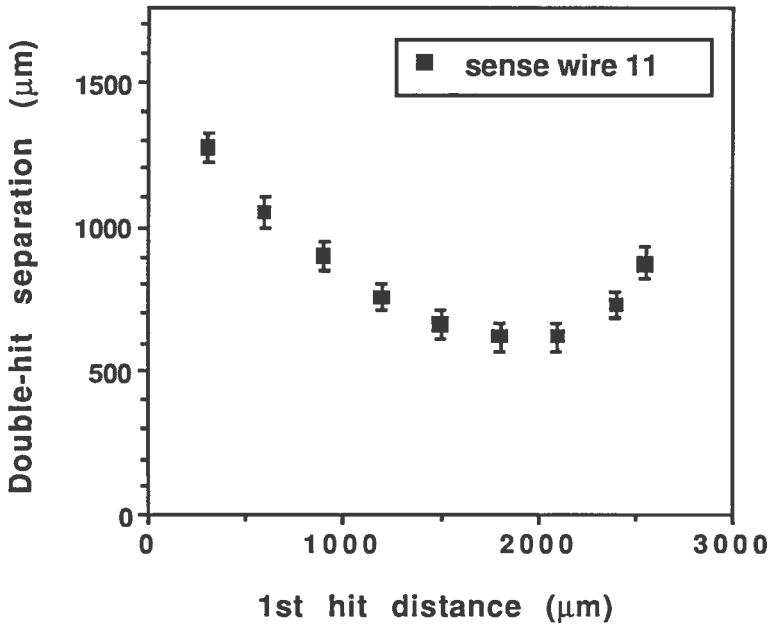

Fig. 21 - Two-hit separation as a function of drift distance of the first hit relative to sense wire 11.

Note that the resolution and the double-hit separation strongly depend on the drift cell electric field configuration. In order to achieve even better detector performances, we have studied a new electric field configuration. The results of this test will be presented in a forthcoming paper.

4. - CONCLUSIONS

The ZEUS vertex detector prototype has given excellent performances; namely a wire efficiency of 96% and a spatial resolution in the central region of the drift space of 35 μm. These characteristics have been checked to be stable with respect to rate, θ and ϕ angles, and along the wire direction.

Computer simulations show that the VXD in the ZEUS experiment will improve significantly, i.e. by a factor of 3, the precision of the measurement of the track impact parameter in the plane transverse to the beam D_0. This is shown via a direct comparison with the resolution in D_0 obtained using only the CTD. The simulations allow a comparison of σ_{D0} as a function of momentum at fixed polar angle θ = 90° (fig. 22a). The improvement in $\sigma_{1/p}$ is shown, at the same value of θ, in fig. 22b. Finally, for two values of momentum p = 1 and 50 GeV/c, the improvement in σ_{D0} is shown as a function of different values of polar angle in figs. 23a and 23b.

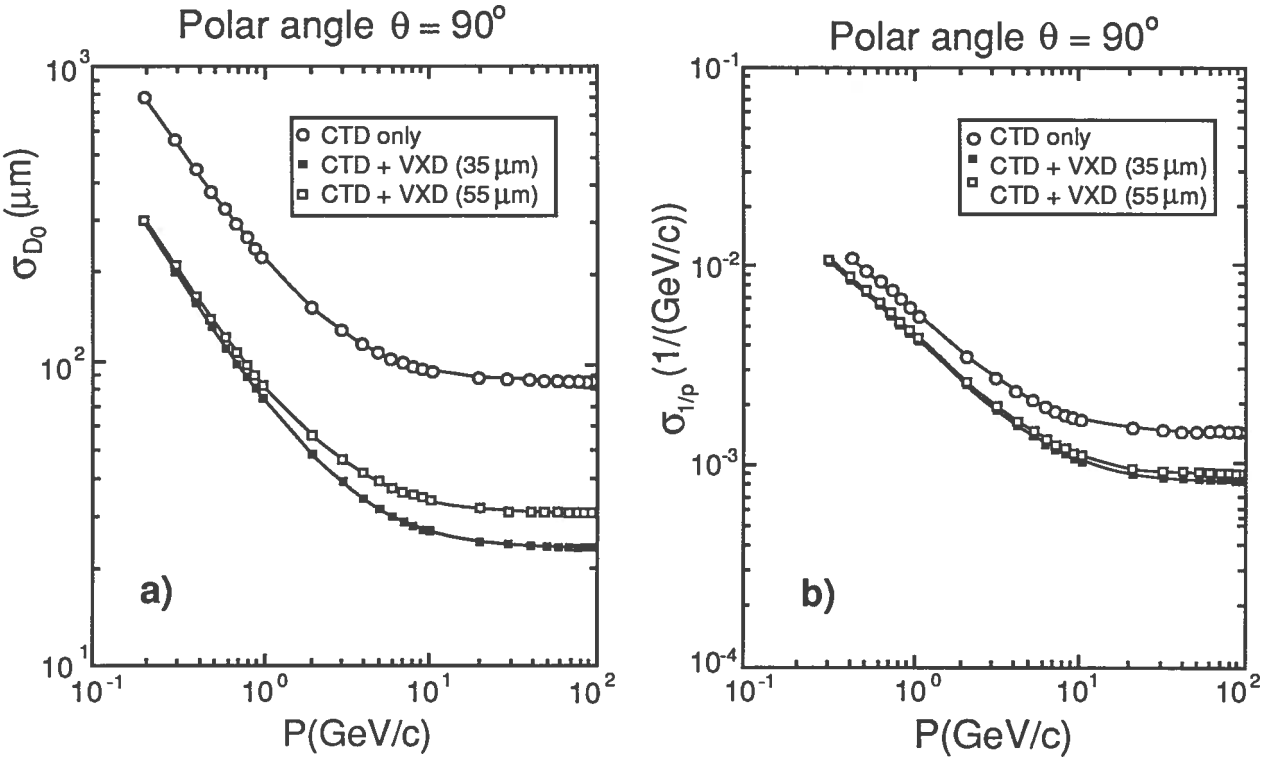

Fig. 22 - The resolutions in D_0 and $1/p$, as obtainable in the ZEUS experiment using the VXD together with the CTD, are shown as functions of momentum at fixed polar angle (respectively a and b). The results refers to two possible values of the VXD resolution: 35 μm and 55 μm. In each plot, the performance of the CTD alone is superimposed.

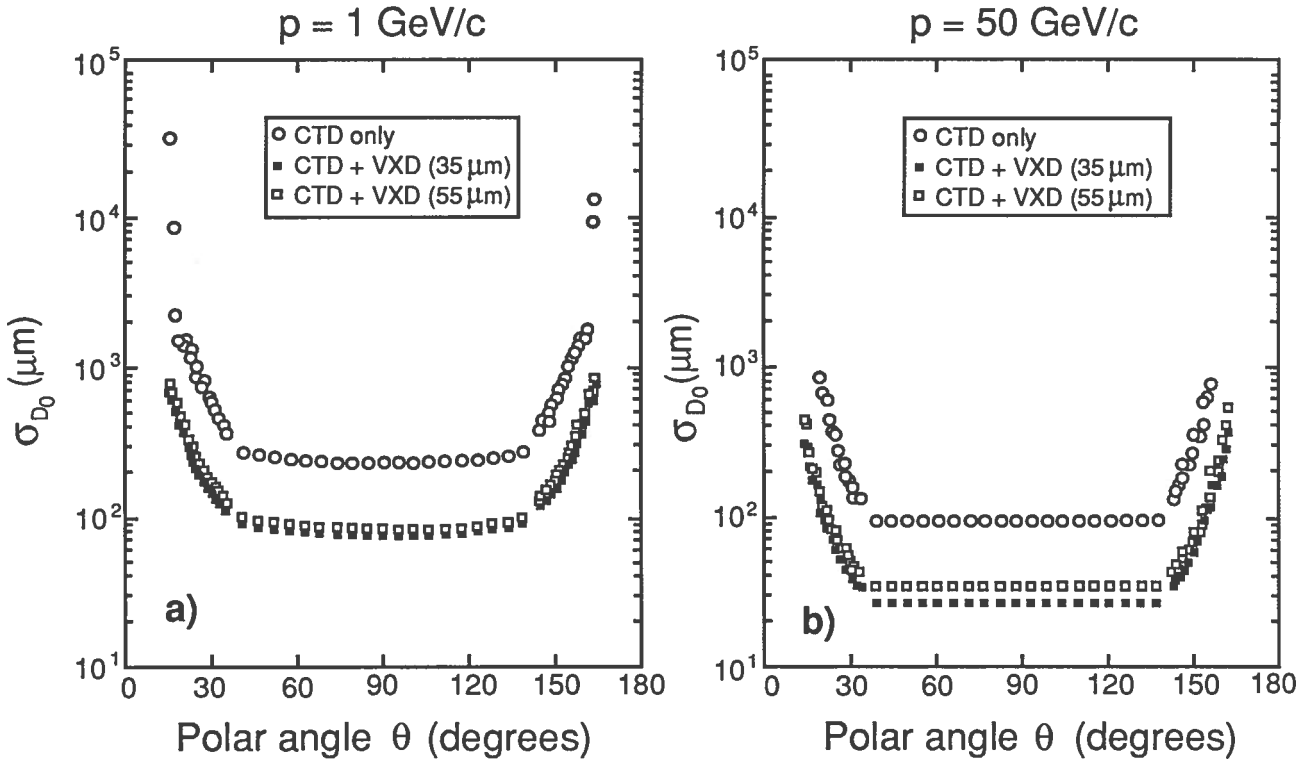

Fig. 23 - The resolution in D_0, as obtainable in the ZEUS experiment using the VXD together with the CTD, is shown as a function of polar angle at 2 values of momentum p = 1 and 50 GeV/c (respectively a and b). The results refers to two possible values of the VXD resolution: 35 μm and 55 μm. In each plot, the performance of the CTD alone is superimposed.

Acknowledgements

We should like to thank the technical staff of the Bologna INFN Section: F. Bugatti, A. Montanari, A. Pieretti, S. Serra, A. Zucchini. We should also like to express our gratitude to A. Gandi for the PC boards, R. Angeloz for the metrological survey, R. Kopp for the copper shielding, H. Bienkowsky for his continuous help, and Prof. F. Villa for his collaboration. Finally, we thank our colleagues from Siegen University for the front-end electronics and for participating in some of the test runs.

REFERENCES

(1) G. Wolf, "HERA: physics, machine and experiments", preprint DESY 86-089.
(2) R.K. Ellis and Z. Kunszt, Nucl. Phys. B303 (1988) 653.
(3) A. Ali et al., "Heavy quark physics at HERA", preprint DESY 88-119.
(4) G. Bari et al., Nucl. Instrum. Methods A239 (1985) 497.
(5) G. Bari et al., Nucl. Instrum. Methods A251 (1986) 292.
(6) J. Va'Vra, Nucl. Instrum. Methods A217 (1983) 322.
(7) The ZEUS Detector Status Report 1989, March 1989.
(8) G. Anzivino et al., "The ZEUS Vertex Detector readout electronics", (in preparation).